ORIGINAL RESEARCH ARTICLE

Understanding Scale-Up of High-Current Electrodes

SVENN ANTON HALVORSEN, EGIL VÅLANDSMYR HERLAND, MANUEL SPARTA, and VETLE KJÆR RISINGGÅRD

A simple and generic model for the heat distribution in electrodes for primary metal production has been investigated. The equations have been analyzed focusing on understanding the scale-up of electrodes under both direct current (DC) and alternating current (AC) conditions. The analysis provides a theoretical foundation for Westly's empirical scale-up rule. For graphite and small carbon electrodes, the current-carrying capacity is limited by the ohmic heating, which controls the lateral heat flux and the temperature at the electrode periphery. For these electrodes, the current capacity is higher for DC than for AC. For large carbon or Søderberg electrodes, the electrode current must be limited to avoid large thermal stresses and subsequent breakages, especially in connection with shutdowns or considerable current fluctuations. Thermally, the current capacity is then limited by the maximum temperature difference between the center and the periphery. For this case, AC electrodes can carry more current than DC.

https://doi.org/10.1007/s11663-023-02811-7

I. INTRODUCTION

METALLURGY has changed from an art into science during the last 150 years. This is not quite the case for the scaling of these processes. In contrast to the chemical industry, where it often is sufficient to go from laboratory to the industrial scale through one intermediate step or directly, the metallurgical industry all too often increases the scale by only a few percent at a time for new processes.[1] Even worse, lack of adequate scale-up know-how has all too frequently resulted in industrial processes that have not worked, or worked with capacities far below the target.[2,3]

In many processes, the required power is generated by resistive heating from large electrical currents supplied through large electrodes. Scale-up implies increased currents, and the type and size of electrodes are key issues that must be addressed for designing and dimensioning such electric furnaces.[4]

SVENN ANTON HALVORSEN, MANUEL SPARTA and VETLE KJæR RISINGGÅRD are with the NORCE Norwegian Research Centre AS, Universitetsveien 19, 4633, Kristiansand, Norway. Contact e-mail: veri@norceresearch.no EGIL VÅLANDSMYR HERLAND is with the NORCE Norwegian Research Centre AS and also with the Elkem ASA Technology, Fiskaaveien 100, 4675, Kristiansand, Norway.

Manuscript submitted October 13, 2022; accepted April 26, 2023.
Article published online June 8, 2023.

The current-carrying capacity of an electrode is limited. It is commonly stated that the maximum current that can be carried by the electrode is given by,[4–9]

$$I = C_e \left(\frac{R_{AC}}{R_{DC}} \right)^{-1/2} D^{3/2}, \quad [1]$$

where R_{AC}/R_{DC} is a factor correcting for the skin and proximity effects, D is the electrode diameter, and C_e is an electrode load factor. This expression is based on a simple, yet powerful power balance argument.[5] The energy generated by resistive heating within the electrode is balanced by the heat transfer to the surrounding material from the surface of the electrode. Increasing the current within the electrode means that the heat transfer and the temperature of the surface increase. In other words, the scaling rule in Eq. [1] is based on the assumption that the current-carrying capacity of the electrode is limited by the resulting electrode surface temperature. A natural consequence of the scaling rule in Eq. [1] is that direct current (DC) electrodes exhibit larger current-carrying capacity than alternating current (AC) electrodes of the same size, since the effective resistance of AC electrodes R_{AC} is larger than the resistance of DC electrodes R_{DC} because of skin and proximity effects. Indeed, many manufactures of graphite electrodes specify larger current-carrying capacities for large DC electrodes compared with AC electrodes of the same size.[10,11]

The scaling rule in Eq. [1] is well established and supported by operational data.[6] The electrode surface temperature is associated with the oxidation rate of carbon material, and this is likely to be an important

mechanism for limiting the electrode consumption in many cases. However, it is also clear that other parameters than the surface temperature may play a role in limiting the current-carrying capacity of electrodes. Many reports highlight thermal stresses and subsequent breakages as important issues, typically in connection with shutdowns or fluctuations in the current.[6,9,12–15] This suggests that temperature gradients or temperature differences within the electrode are important for the current-carrying capacity. Other mechanisms that might play a role are the chemical composition of surrounding material,[7] and the grade or quality of the electrode material.[7,14]

The purpose of this work is to study how the current-carrying capacity is limited for large electrodes, including differences between AC and DC. Two different scale-up criteria will be discussed. The results are derived by analyzing a fairly simple thermal model for an electrode. In Section II, the model is described and analyzed. The consequences for scale-up of the current-carrying capacity are investigated in Sections III and IV. The final discussion and conclusions can be found in Sections V and VI.

II. ELECTRODE MODEL

This work considers the simplified electrode geometry shown in Figure 1. The electrode is modeled as a cylinder with radius R and length L. A total electric current I is flowing in the cylinder, and the important material properties are the electrical conductivity σ, thermal conductivity k, and magnetic permeability μ. The ambient temperature is assumed to be T_a, and the electrode exchanges heat with the ambient material with an effective heat-transfer coefficient h. The effective heat-transfer coefficient captures the sum of all mechanisms that dissipate heat, see Section II–B.

For the purpose of understanding electrode scale-up with temperature-related scale-up criteria, the heat equation must be solved for the electrode system. The heat equation describes the temperature field $T(\mathbf{r}, \mathbf{t})$ as a function of space and time, and it reads

$$\rho c_p \frac{\partial T}{\partial t} + \rho c_p v_z \frac{\partial T}{\partial z} = \nabla \cdot (k \nabla T) + p, \qquad [2]$$

where ρ is the mass density, c_p is the specific heat capacity, and p is the power generated per unit volume. The quantity v_z is the average downwards slipping rate. It is assumed that the electrode is slipped regularly, in very small steps, and that the effect of this motion can be averaged. For simplicity, it is also assumed that all material properties are constant. This approximation is suitable for developing a basic understanding of the problem.

A. *Power Distribution in AC Electrodes*

In electrodes, the term p accounts for the resistive heating caused by the current. The power density is given by

$$p = \frac{|\mathbf{J}|^2}{\sigma}, \qquad [3]$$

where $\mathbf{J}$ is the current density, which can be expressed in terms of the electric field $\mathbf{E}$ as $\mathbf{J} = \sigma \mathbf{E}$ using Ohm's law. In AC electrodes, $\mathbf{J}$ oscillates with a frequency f. Hence, in the following, p should be understood as time-averaged resistive power density and $|\mathbf{J}|$ as the root-mean-squared current density magnitude when AC electrodes are considered. The AC current density in electrodes for three-phase electric furnaces has been reviewed in Reference 16. Relevant results can also be found in standard textbooks, such as References 17 and 18.

Ignoring the effects close to the top and bottom of the electrode, the current will flow vertically. The distributions of the current and the relative resistance and reactance are determined by the nondimensional ratio R/δ, where δ is the skin depth, defined as

$$\delta = \sqrt{\frac{1}{\pi f \mu \sigma}}. \qquad [4]$$

In this section, we give a short summary of some of the main properties of the current distribution. Details and references can be found in Reference 16.

Figure 2 shows that a uniform distribution of the current (DC solution) is obtained for $R/\delta = 0$ (see Supplementary Material for the code used to produce the figures). This is also a very good approximation for small values, $R/\delta \ll 1$. Deviations from a uniform distribution are significant for $R/\delta = 2$ and increase for larger values of R/δ. For very large values, all of the current will be concentrated in a thin layer on the periphery of the electrode with characteristic thickness δ. This is known as the *skin effect*.

Figure 3 reveals two different regimes for the total resistance of the electrode. For $R/\delta < 1$, the DC resistance is an appropriate approximation. In this regime, the electrode resistance scales in the same manner for both AC and DC, *i.e.*, $R_{AC} \sim R^{-2}$ and $R_{DC} \sim R^{-2}$. For $R/\delta > 2$, the ratio of the AC to the DC resistance increases more or less linearly with R/δ. Analyzing the asymptotics reveals that $R_{AC}/R_{DC} \sim R/\delta$ for large values of R/δ, which implies that $R_{AC} \sim R^{-1}$. Clearly, the nondimensional parameter R/δ plays an important role for dimensioning and scale-up of electrodes.

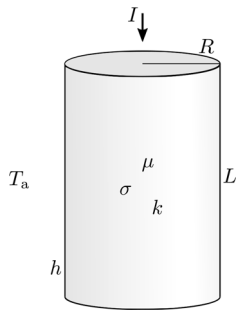

Fig. 1—Figure of model geometry. Important material properties and physical and geometrical parameters are denoted in the figure.

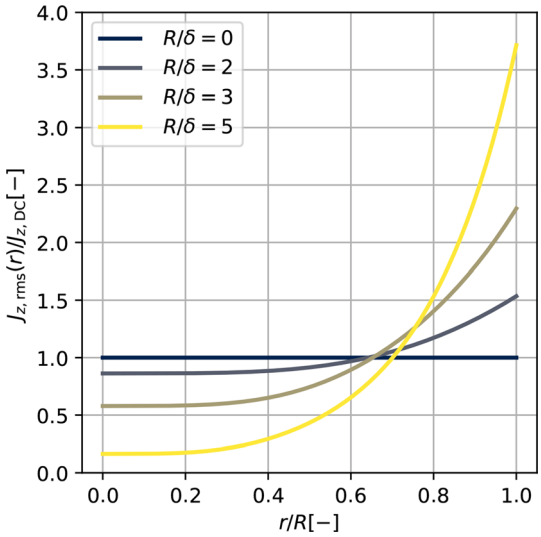

Fig. 2—Radial current distribution for different values of the nondimensional parameter R/δ. The x-value is the nondimensional radius r/R. The y-value is the nondimensional current density $J_{z,\mathrm{rms}}(r)/J_{z,\mathrm{DC}}$, which is normalized by the spatially uniform DC current density. $R/\delta = 0$ corresponds to the DC limit.

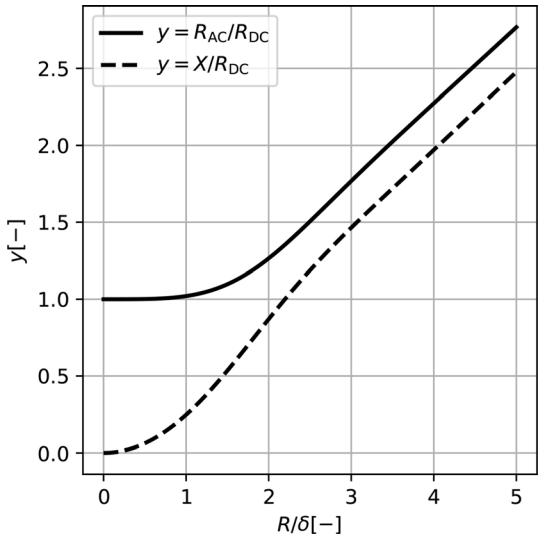

Fig. 3—The skin effect factor R_{AC}/R_{DC} and reactance factor X/R_{DC} as a function of nondimensional parameter R/δ.

We also note that the same inductive effects that cause the skin effect yield a nonzero reactance for $R/\delta > 0$. The nondimensional reactance X/R_{DC} is, as shown in Figure 3, low or moderate when $R/\delta < 1$, and increases linearly for $R/\delta > 2$, in the same fashion as R_{AC}/R_{DC}. Accounting for both resistive and inductive effects, Figure 3 shows that AC effects can be significant when $R/\delta > 1$.

Typical values for the frequency f, electrical conductivity σ, and the resulting skin depth δ for electrodes are shown in Table I. The relative magnetic permeability is assumed to be 1, *i.e.*, $\mu = \mu_0 = 4\pi \cdot 10^{-7}$H/m. Hence, AC effects cannot be ignored for graphite electrodes with diameters greater than some 0.3 m, and for carbon or Søderberg electrodes with diameters above some 0.9 m.

Table I. Typical Values for the Frequency f, Electrical Conductivity σ , and the Resulting Skin Depth δ for Graphite, Carbon, and Søderberg Electrodes

	f (Hz)	σ (S/m)	δ (m)
Graphite	60	2.5×10^5	0.13
Carbon	50	2.8×10^4	0.43
Søderberg	50	2.5×10^4	0.45

Values for the electrical conductivity are based on Refs. [10], [11], and [19].

B. *Heat Equation for Axisymmetric Electrode*

In order to solve Eq. [2] for the electrode in Figure 1, we assume quasi-stationary conditions and axial symmetry. The heat equation can then be written as

$$-\rho c_p v_z \frac{\partial T}{\partial z} + \frac{1}{r}\frac{\partial}{\partial r} rk \frac{\partial T}{\partial r} + \frac{\partial}{\partial z} k \frac{\partial T}{\partial z} + p = 0. \qquad [5]$$

These assumptions imply that the power distribution and the boundary conditions do not change with time and that initial transients have died out. Furthermore, they also imply that there is no dependence on the azimuthal angle ϕ in the boundary conditions and the power density.

An appropriate and relevant boundary condition suitable for electrodes is convective heat transfer,

$$\mathbf{n} \cdot \mathbf{q} = h(T - T_a), \qquad [6]$$

where $\mathbf{n}$ is the boundary normal, $\mathbf{q} = -k\nabla T$ is the heat flux, h is the heat-transfer coefficient, and T_a is the ambient temperature. Convective heat transfer is the standard boundary condition for solid–fluid interfaces. However, other boundary conditions can also be expressed in this rather general form. Ambient radiation, with $\mathbf{n} \cdot \mathbf{q} = \epsilon\sigma_{SB}(T^4 - T_a^4)$, where ϵ is the emissivity and σ_{SB} is the Stefan–Boltzmann constant, can be written as $\mathbf{n} \cdot \mathbf{q} = h(T - T_a)$, with a temperature-dependent heat-transfer coefficient $h = \epsilon\sigma_{SB}(T^2 + T_a^2)(T + T_a)$. A thermally resistive layer can also be written as $\mathbf{n} \cdot \mathbf{q} = h(T - T_a)$, with $h = k_l/d_l$ where k_l is the thermal conductivity and d_l is the thickness of the layer. In addition to the convective boundary condition at the surface of the electrode, the condition

$$\left.\frac{\partial T}{\partial r}\right|_{r=0} = 0, \qquad [7]$$

is imposed on the axis, due to axial symmetry.

The next step of the analysis is to introduce the nondimensional variables $r = R\tilde{r}$, $z = L\tilde{z}$, and $T = T_0 + (T_m - T_0)\tilde{T}$, where T_0 and T_m are the minimum and maximum temperatures of the system, such that the nondimensional temperature $\tilde{T} \in [0, 1]$ throughout the system. Inserted in Eq. [5], the result is

$$-\frac{R^2\rho c_p v_z}{Lk}\frac{\partial\tilde{T}}{\partial\tilde{z}} + \frac{1}{\tilde{r}}\frac{\partial}{\partial\tilde{r}}\tilde{r}\frac{\partial\tilde{T}}{\partial\tilde{r}} + \left(\frac{R}{L}\right)^2\frac{\partial^2\tilde{T}}{\partial\tilde{z}^2} + \frac{R^2}{k\Delta T}p(R\tilde{r}) = 0, \quad [8]$$

where $\Delta T = T_m - T_0$.

We note that there is a quadratic dependence on the aspect ratio R/L in the third term. When $R \leq L/3$, this ratio is small, and the third term can be neglected as a first approximation,

$$-\frac{R^2\rho c_p v_z}{Lk}\frac{\partial\tilde{T}}{\partial\tilde{z}} + \frac{1}{\tilde{r}}\frac{\partial}{\partial\tilde{r}}\tilde{r}\frac{\partial\tilde{T}}{\partial\tilde{r}} + \frac{R^2}{k\Delta T}p(R\tilde{r}) = 0. \quad [9]$$

In the following, we will assume that the Péclet number,

$$Pe = \frac{R^2\rho c_p v_z}{Lk}, \quad [10]$$

is small, and hence the first term in Eq. [8] can be neglected. This Péclet number measures the relative importance of the *vertical* advective heat transport by slipping, and the *horizontal* heat transport by conduction. Note that this definition differs from the usual one, in which advection and diffusion take place along the *same* axis. However, our definition is consistent with the assumption $R \leq L/3$, which implies that vertical heat conduction is negligible compared to horizontal heat conduction. The assumption of a small Péclet number will be discussed in more detail in Section V.

The assumptions $R \leq L/3$ and $Pe < 1$ give the second-order nonhomogeneous ordinary differential equation

$$\frac{1}{\tilde{r}}\frac{\mathrm{d}}{\mathrm{d}\tilde{r}}\tilde{r}\frac{\mathrm{d}\tilde{T}}{\mathrm{d}\tilde{r}} + \frac{R^2}{k\Delta T}p(R\tilde{r}) = 0. \quad [11]$$

The boundary condition in Eq. [6] is also conveniently expressed in nondimensional form,

$$\left.\frac{\mathrm{d}\tilde{T}}{\mathrm{d}\tilde{r}}\right|_{\tilde{r}=1} = -Bi\left[\tilde{T}(\tilde{r}=1) - \tilde{T}_a\right], \quad [12]$$

where $Bi = hR/k$ is the dimensionless Biot number. The Biot number quantifies the importance of internal *vs* surface heat-transfer resistance of an object.[20] A small value of Bi means that thermal resistance within the object is small, compared with the surface thermal resistance. Consequently, the temperature within the body is relatively uniform. This often allows for lumped system analysis of thermal components. A large value of Bi means that the thermal resistance associated with the surface is small. In that case, the temperature difference associated with the surface is small compared with the temperature differences in the interior of the body.

Some typical values for the Biot and Péclet numbers are given in Table II. The low values for the heat-transfer coefficient correspond roughly to an electrode at 800 °C radiating against surroundings at 500 °C, while the high value corresponds to an electrode surface at some 1600 °C and an ambient temperature of 1400 °C. An effective emissivity of 0.8 is assumed in both cases.

Reliable temperature-dependent material data for Søderberg paste and baked electrodes have not been published, though room-temperature values are available for raw paste and paste baked at 1000 °C. In Reference 19, Elkem published an analysis of the Persson-type composite electrode, including a comparison of different types of electrode paste. We consider these values sufficiently accurate to provide indicative values for the Biot and Péclet numbers and have used these values for calculating the Biot and Péclet numbers for graphite and Søderberg electrodes in Table II. For carbon electrodes, we have assumed a somewhat higher heat conductivity than for Søderberg electrodes and set the density and the specific heat capacity to the average of the graphite and Søderberg values. Finally, the electrode length is set to 3 m and a relatively high slipping rate of 1 m/d has been assumed.

The examples in Table II suggest that the Biot number is typically small to moderate for graphite electrodes, and moderate to large for carbon and Søderberg electrodes. The values will definitely be large ($Bi > 10$) for large high-current carbon or Søderberg electrodes. The values of the Péclet number indicate that the corresponding term can be neglected in Eq. [8] as a first approximation. We will make further comments for the case of large Søderberg electrodes in Section V.

The combined thermal and electromagnetic model of the electrode has now been reduced to solving Eq. [11] with the boundary condition in Eq. [12] and the power density given by the electromagnetic problem. Such a system has been studied before, for instance, by References 21 through 23. We review it here in the context of electrodes. Multiplying both sides of Eq. [11] with $\tilde{r}$ and integrating yields

$$\tilde{r}\frac{\mathrm{d}\tilde{T}}{\mathrm{d}\tilde{r}} = -\int \mathrm{d}\tilde{r}\frac{R^2\tilde{r}}{k\Delta T}p(R\tilde{r}). \quad [13]$$

The integration constant can be determined by using the boundary condition in Eq. [7]. This gives, with dimensions reintroduced

$$q_r = \frac{1}{r}\int_0^r \mathrm{d}r' r' p(r'). \quad [14]$$

This is obviously the steady-state power balance, where the heat flux q_r at radius r equals the power per unit length generated inside r divided by the circumference.

Table II. Typical Values for the Heat-Transfer Coefficient h, the Thermal Conductivity k, the Density ρ, the Specific Heat Capacity c_p, the Electrode Radius R, and the Resulting Biot Number Bi, and Péclet Number Pe for Large Graphite, Carbon, and Søderberg Electrodes

	h $\left(\frac{W}{m^2K}\right)$	k $\left(\frac{W}{mK}\right)$	ρ $\left(\frac{kg}{m^3}\right)$	c_p $\left(\frac{J}{kg\ K}\right)$	R (m)	Bi (–)	Pe (–)
Graphite, Low Bi	150	90	1700	1900	0.1	0.17	0.0014
Graphite, High Bi	1000	90	1700	1900	0.3	3.3	0.012
Carbon, Low Bi	150	15	1530	1850	0.2	2.0	0.029
Carbon, High Bi	1000	15	1530	1850	0.6	40	0.26
Søderberg, Low Bi	150	8	1360	1800	0.3	5.6	0.11
Søderberg, High Bi	1000	8	1360	1800	0.9	113	0.96

Values for the material properties are based on Ref. [19]. A slipping rate of 1 m/d and an electrode length of 3 m have been assumed for the Péclet number.

The integral on the right-hand side of Eq. [14] can be evaluated and the heat flux can be written as

$$q_r(r) = \frac{R_{AC}}{R_{DC}} g_q(r) q_{R,DC}. \quad [15]$$

The details of this calculation can be found in Appendix VII–A. In Eq. [15], $g_q(r)$ is a shape function ranging from 0 at $r = 0$ to 1 at $r = R$, and

$$q_{R,DC} = \frac{I_{rms}^2}{2\pi^2 \sigma R^3}, \quad [16]$$

is the boundary heat flux for the DC case.

The temperature can now be found by integrating Eq. [15], using the boundary condition in Eq. [12] to determine the integration constant. The internal temperature can be written as the sum of three terms:

$$T(r) = T_a + \Delta T_{surf} + \Delta T_{int}(r), \quad [17]$$

where

$$\Delta T_{surf} = T(R) - T_a = \frac{2}{Bi} \frac{R_{AC}}{R_{DC}} \Delta T_{max,DC}, \quad [18]$$

is the temperature difference between the electrode surface and the ambient and

$$\Delta T_{int}(r) = T(r) - T(R) = g_T(r) \Delta T_{max,DC}, \quad [19]$$

is the temperature variation in the interior of the electrode. $g_T(r)$ is a shape function that is 0 at the periphery (where $r = R$) and that is determined in Appendix VII–B. In Eqs. [18] and [19], $T(R)$ is the electrode surface temperature, whereas the factor

$$\Delta T_{max,DC} = \frac{I_{rms}^2}{4\pi^2 \sigma k R^2} \quad [20]$$

is the temperature difference between the electrode center and surface in the DC case.

The two shape functions, $g_q(r)$ and $g_T(r)$, can be written in terms of two nondimensional numbers, R/δ and r/R. Thus, the radial profiles of q_r and ΔT_{int} are determined by R/δ only.

C. *Properties of the Solution*

For $R/\delta \ll 1$, we recover the DC limit of the solution. In this limit.

$$\frac{R_{AC}}{R_{DC}} = 1 \quad [21]$$

and

$$g_q(r) = \frac{r}{R}. \quad [22]$$

This gives the heat flux

$$q_r(r) = q_{R,DC} \cdot \frac{r}{R}. \quad [23]$$

Furthermore,

$$g_T(r) = 1 - \left(\frac{r}{R}\right)^2, \quad [24]$$

giving

$$\Delta T_{int}(r) = \Delta T_{max,DC} \cdot \left[1 - \left(\frac{r}{R}\right)^2\right], \quad [25]$$

Further details, including correction terms for small values of R/δ, are given in Appendix VII–C.

The normalized internal temperature distribution $\Delta T_{int}/T_{max,DC}$ and normalized heat flux $q_r/q_{R,DC}$ are shown in Figure 4 as functions of r/R for $R/\delta \in \{0, 2, 3, 5\}$. As expected based on equations Eqs. [23] and [25], q_r is linear and ΔT_{int} is quadratic in the DC limit. With a significant skin effect, q_r and ΔT_{int} change abruptly close to the electrode surface, whereas there is almost no heat flux and approximately constant temperature in the center of the electrode, where there are insignificant amounts of current. Even though more power is generated in the electrode with increasing skin effect, the temperature difference between the central region and the surface actually decreases, since more of the power is generated close to the surface of the electrode. Comparing an AC and a DC electrode with same size, current, and material, the model shows that the AC electrode will generate more power and have a

larger heat flux at the surface, while the DC electrode will exhibit a larger temperature difference between the center and the periphery.

The temperature inside the electrode is determined by two nondimensional numbers, namely the Biot number Bi and R/δ. We consider the effect of each of these in Figure 5. Figure 5 shows the ratio of the temperature difference between the electrode surface and the ambient and the center and the ambient. Note the definition of ΔT_{surf} in Eq. [18] and the definition

$$\Delta T_{\text{total}} = \Delta T_{\text{surf}} + \Delta T_{\text{int}}(0) = T(0) - T_a. \qquad [26]$$

Clearly, ΔT_{surf} dominates for small Biot numbers, $Bi < 0.1$, whereas temperature variations within the electrode dominate for large values of Bi, *e.g.*, $Bi > 100$. Between these extreme values, R/δ has a comparatively strong influence.

The ratio $\Delta T_{\text{surf}}/\Delta T_{\text{total}}$ depends on R/δ through ΔT_{surf} and $\Delta T_{\text{int}}(0)$. ΔT_{surf} depends on R/δ through the skin effect factor $R_{\text{AC}}/R_{\text{DC}}$. Consequently, the dependence of ΔT_{surf} on R/δ is the same as for $R_{\text{AC}}/R_{\text{DC}}$ in Figure 3, except for a constant multiplier $2\Delta T_{\text{max,DC}}/Bi$. It follows that the electrode surface temperature, $T(R)$, increases with R/δ. $\Delta T_{\text{int}}(0)$ depends on R/δ through $g_T(0)$, which decreases with increasing values of R/δ. This gives a further boost to $\Delta T_{\text{surf}}/\Delta T_{\text{total}}$ as a function of R/δ.

The temperature inside the electrode relative to the ambient, $T(r) - T_a$, is shown in Figure 6 for three different values of the Biot number and four different values of R/δ. These graphs are suitable for studying the combined contributions of ΔT_{surf} and ΔT_{int}. ΔT_{surf} enters the graph as the y-value at $r/R = 1$, whereas ΔT_{int} is responsible for the temperature variation in the interior of the electrode. For small values of Bi, the temperature is to a large extent determined by ΔT_{surf}, and increasing R/δ gives a large temperature increase. Under such conditions, the temperature of the electrode is approximately proportional to the skin effect factor $R_{\text{AC}}/R_{\text{DC}}$. On the other hand, for large values of Bi, ΔT_{surf} is small, and the temperature is dominated by temperature differences within the electrode. Consequently, the temperatures in the center of the electrode decreases with a stronger skin effect, even though the amount of power generated in the electrode increases as R/δ.

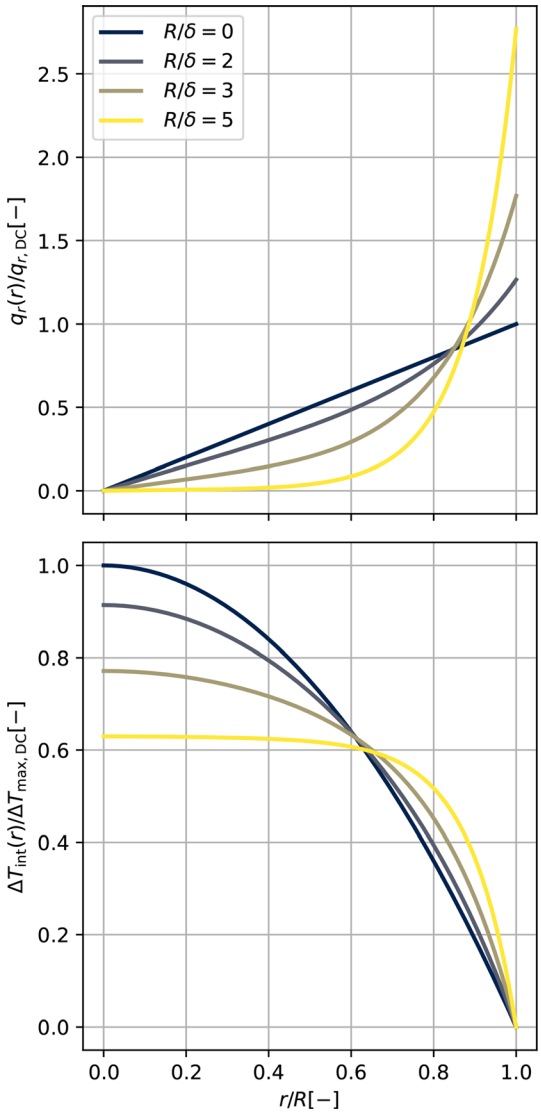

Fig. 4—Normalized (nondimensional) radial heat flux and temperature profiles for different values of R/δ.

III. CONSEQUENCES FOR SCALE-UP

The following thermal criteria may limit the current-carrying capacity of an electrode:

- the temperature at the periphery
- the heat flux at the periphery
- internal temperature differences
- the maximum temperature

Obviously, an electrode's current-carrying capacity is also limited by other factors, such as electrode quality, type of process, process conditions, and so on. However, these factors remain unchanged during scale-up, and understanding heat flow and temperatures is therefore of central importance.

A. *Maximum $T(R)$ or $q_r(R)$*

As a first approximation, we assume that T_a does not change during scale-up. Thus, for the model discussed here, the first two criteria are equivalent as the surface temperature determines the heat flux through Eq. [6].

Since the shape function in Eq. [15] is 1 at $r = R$, the heat flux at the electrode periphery can be written as

$$q_r(R) = \frac{R_{\text{AC}}}{R_{\text{DC}}} \frac{I_{\text{rms}}^2}{2\pi^2 \sigma R^3}. \qquad [27]$$

Setting $q_r(R) = q_{R,\text{max}}$ and solving for I_{rms} give the maximum electrode current as

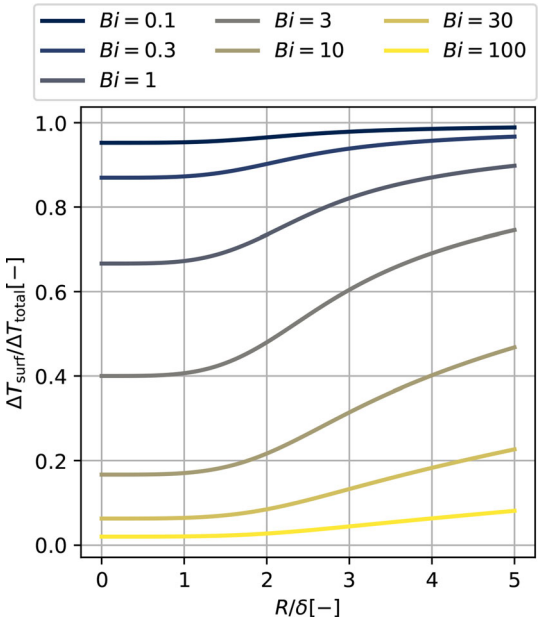

Fig. 5—Ratio between the surface temperature difference and total temperature difference, $\Delta T_{\text{surf}}/\Delta T_{\text{total}}$.

$$I_{\text{rms}} = C_e \left(\frac{R_{\text{AC}}}{R_{\text{DC}}} \right)^{-1/2} D^{3/2}, \qquad [28]$$

where $D = 2R$ is the electrode diameter,

$$C_e = \frac{\pi}{2} \sqrt{\sigma q_{R,\max}} \qquad [29]$$

is the electrode load factor, and $q_{R,\max}$ is the upper limit for the boundary heat flux. Alternatively, the electrode load factor can be written in terms of the maximum temperature at the periphery:

$$C_e = \frac{\pi}{2} \sqrt{(T_{R,\max} - T_a)\sigma h}. \qquad [30]$$

Interestingly, this scale-up criterion reproduces Westly's scaling rule.[6,7] Since $R_{\text{AC}}/R_{\text{DC}} = 1$ in the DC limit and increases as R/δ for strong skin effects, it follows that $I_{\text{rms}} \propto D^{3/2}$ for small electrodes where skin effects are insignificant, whereas $I_{\text{rms}} \sim D$ for large electrodes with significant skin effects.

B. *Maximum* $\Delta T_{\text{int,max}}$

For large electrodes, the current must be limited to avoid excessive thermal stresses and subsequent breakages, especially in connection with shutdowns or considerable current fluctuations.[6,9,12–15] Thermal stresses are caused by large temperature differences, cf. Section IV. Thus, this places an upper limit on the internal temperature difference,

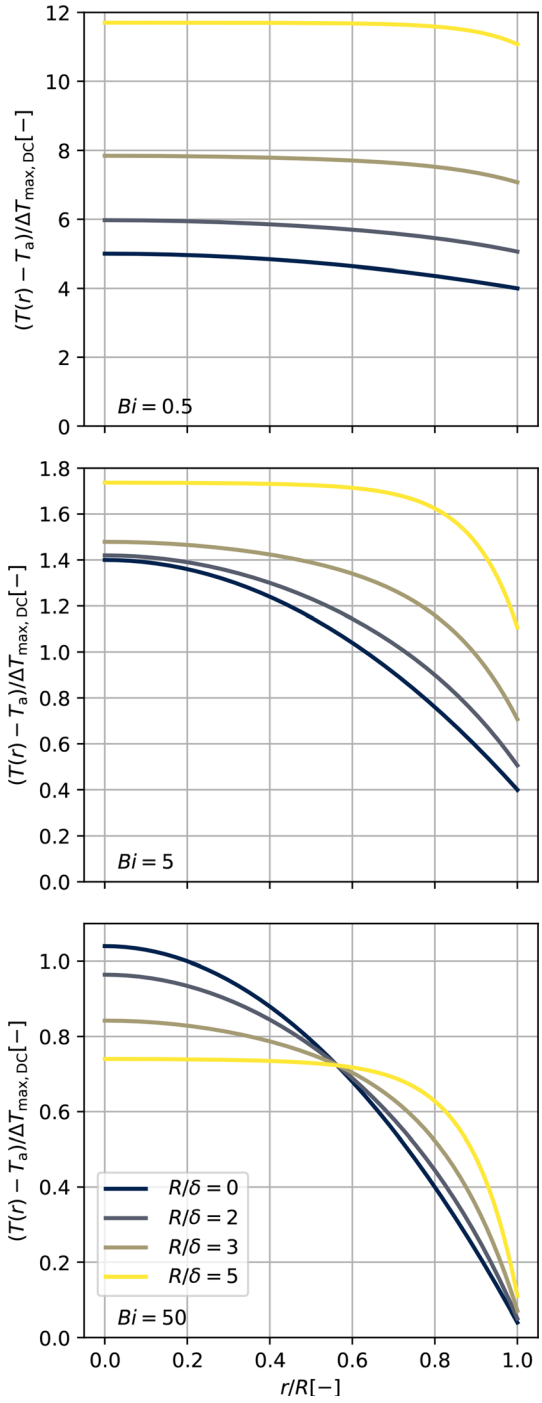

Fig. 6—Normalized temperature profiles as a function of r/R.

$$\Delta T_{\text{int,max}} = \Delta T_{\text{int}}(0) = g_T(0) \Delta T_{\text{max,DC}}. \qquad [31]$$

Using Eq. [20], this criterion can be written as

$$\Delta T_{\text{int,max}} = g_T(0) \frac{I_{\text{rms}}^2}{4\pi^2 \sigma k R^2}. \qquad [32]$$

Hence, the maximum current scales as

$$I_{\text{rms}} = CD, \qquad [33]$$

where

$$C = \pi \sqrt{\sigma k \frac{\Delta T_{\text{int,max}}}{g_T(0)}}. \quad [34]$$

This is in agreement with Westly's scaling rule for large electrodes.[6,7]

The maximum current for large electrodes will be proportional to the diameter both in the DC limit and for electrodes with a significant skin effect. The value of the shape function g_T at the center of the electrode, $g_T(0) = \Delta T_{\text{int,max}}/\Delta T_{\text{max,DC}}$, is plotted as a function of R/δ in Figure 7. The shape function is 1 in the limit $R \ll \delta$. For $R \gg \delta$, the shape function approaches a constant value between 0.5 and 0.6. Consequently, the constant of proportionality C is larger for AC electrodes than for DC electrodes.

C. *Maximum T_{max}*

The maximum temperature will occur at the centerline of the electrode. At extreme temperatures, carbon can vaporize. To our knowledge, this has not been reported as a problem, and we see no reason why it should be. Potential problems due to high temperature will be connected to the temperature at, or close to, the surface. Here, the electrode can react with the ambient gas, liquids, or solids.

One possible exception is an electrode with a central hole. Electrodes with a central hole are not considered in this work, but if the hole is small compared to the electrode diameter, our model can be applied as a first approximation.

IV. THERMAL STRESSES

A comprehensive analysis of mechanical stress in electrodes is out of the scope for this work. However, in this section, we discuss some basics related to scale-up limited by internal temperature differences in the electrodes.

The thermal strain tensor is given by Reference 24

$$(e_T)_{ij} = \alpha \Delta T_{\text{stress}} \delta_{ij}, \quad [35]$$

where $(e_T)_{ij}$ is the strain tensor, α is the coefficient of thermal expansion, ΔT_{stress} is the difference between the local temperature and a temperature where there is no thermal stress, and δ_{ij} is the Kronecker delta. The strain tensor describes the unrestricted local material deformation. Starting from a stress-free state at a constant temperature, a change in temperature will give rise to uniform expansion or contraction in all directions if the external forces acting on the material are negligible. However, if there are internal temperature gradients within the material, each point will try to expand or contract according to the *local* value of the thermal strain. Incommensurate strains at different points will give rise to thermal stresses.

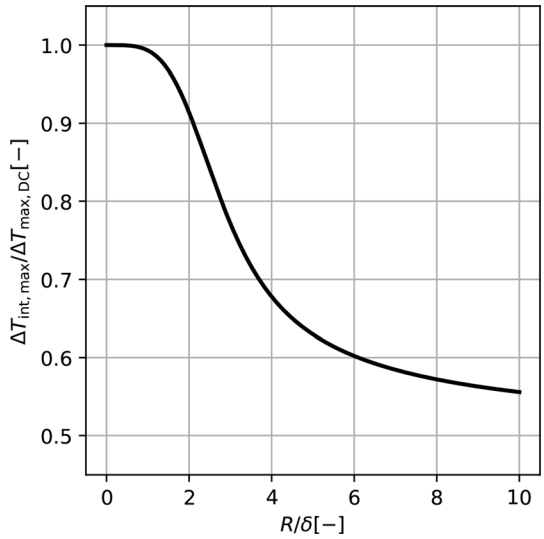

Fig. 7—Normalized center to surface temperature difference $\Delta T_{\text{int,max}}$ as a function of R/δ.

Now consider a large electrode with constant material properties. We assume that the electrode is free to expand in the r direction, and r stress and hoop stress are neglected. In other words, we only consider vertical stress. We further assume that the entire electrode can expand freely in the vertical direction. Each cross section of the electrode must, however, *remain as a cross section*. In regions with thermal strain larger than the weighted average, the electrode is prevented from expanding vertically, which gives rise to compressive stress. Similarly, in regions with thermal strain below the average, the material will have to expand more than dictated by the local temperature, resulting in tensile stress.

For a large electrode with a large Biot number, there will be considerable temperature differences on every cross section. In the center, where the highest temperatures are found, the thermal strain will be largest, and the stress will be compressive. At the periphery, where the temperatures are lower, the thermal strain is less, and the stress will be tensile. The tensile stress on the periphery arising by this mechanism can be shown to be significantly larger than the tensile strength at normal operation. However, since electrodes normally do not break, this stress must be relieved. Since baked carbon is a brittle material, the most likely mechanism is some form of cracking—either microcracks, or larger horizontal cracks that penetrate only a limited distance into the electrode. Figure 6 shows that the temperature differences inside the electrode are larger for DC currents than for AC currents. The region where tensile stresses must be relieved is therefore larger for DC than for AC. For $R/\delta \gg 1$, stress only needs to be relieved in a comparatively small layer close to the electrode surface in the AC case.

In the following, we assume that the stress release is complete, in the sense that the electrode is stress-free during normal operation. If the current is turned off, the electrode will start cooling. As the electrode cools, the center will try to contract more than the periphery,

giving rise to a reversal of the stress condition, with tensile stress in the center and compressive stress on the periphery. The tensile stress may be relieved by the same mechanisms as before, but since the electrode is already weakened by cracks along the periphery, cracks in the center may penetrate across the entire cross section, giving rise to a hard electrode breakage. By the same argument as for normal operation, DC electrodes need more stress release and are therefore more vulnerable to breakage than AC electrodes (assuming the same effective electrode current).

The above discussion is rather simplistic but reveals that large DC electrodes will be more vulnerable to hard breakages than AC electrodes. Far more detailed calculations are needed in order to investigate the strategies for avoiding breakages and to analyze the conditions for real furnaces. Such calculations have been carried out by Elkem Carbon based on the assumption that the electrode is stress-free during normal operation.[12,13,15]

V. DISCUSSION

In this work, we have intentionally chosen a very simplified model in order to derive analytical expressions that provide insight into electrode scale-up. We have shown that the relevant equations depend on four nondimensional numbers: The Biot number, *Bi*, a Péclet number, *Pe*, describing the relative importance of *vertical* advective heat transport by slipping, *vs horizontal* heat transport by conduction, the squared aspect ratio, $(R/L)^2$, and the relative size of the skin depth, (R/δ). The electrical and thermal conditions of the electrode will be very different depending on whether these numbers are very small, moderate, or very large. Further analysis relating to the role of the skin depth can be found in Reference 25.

The relative importance of vertical *vs* horizontal heat conduction is determined by the squared aspect ratio $(R/L)^2$. As stated in relation to Eq. [8], the condition $R \leq L/3$ is usually fulfilled, meaning that the squared aspect ratio is small and that vertical heat conduction can be neglected. For large AC electrodes, for which R approaches $L/3$, the power is concentrated in a peripheral skin layer of thickness δ. The relevant length scale of horizontal heat conduction is then across the skin layer, rather than across the entire electrode radius. The ratio $(\delta/L)^2$ is then more appropriate than $(R/L)^2$ when comparing horizontal *vs* vertical heat conduction. Hence, the skin effect enhances the importance of horizontal heat conduction.

This is also true when comparing the relative importance of horizontal heat conduction and vertical heat advection using the Péclet number. Table II shows that the Péclet number can approach one for large Søderberg electrodes if R is taken to be the relevant length scale for horizontal heat conduction. However, as shown in Table I, $\delta \approx R/2$ for large Søderberg electrodes, giving a Péclet number comfortably smaller than one if δ is taken to be the relevant length scale. Hence, in a simplified model, such as the one considered here, it is appropriate to cancel the advective term, even for large Søderberg electrodes.

We have considered the thermal model defined by Eq. [11] with the boundary condition of Eq. [12]. This model describes a balance between the electric power deposited in the electrode and horizontal heat conduction. Fundamentally, this is the same basic heat balance that was considered by Andreae,[5] except that Andreae only considered the temperature at the electrode surface, or in other words, the behavior at low Biot numbers. We have used the power distribution within the electrode to compute the temperature variation across the electrode for both direct and alternating currents. By doing so, we have extended Andreae's model across the spectrum from low to high Biot numbers and shown that large temperature differences are more likely to limit the electrode current for high Biot numbers.

Consider first graphite electrodes, which are characterized by a small to moderate Biot number, c.f. Table II. As can be seen from Figure 6, internal temperature gradients are small in this case, whereas there can be a significant temperature difference between the electrode surface and the surroundings. This temperature difference will determine the maximum current for an electrode in a given environment. Hence, maximum $T(R)$ is the appropriate scale-up criterion for small Biot numbers. Figure 6 also shows that the temperature difference between the electrode surface and the ambient is smaller for DC than for AC for a given effective current because more power is generated in the AC case. Hence, manufactures of graphite electrodes can safely specify larger current-carrying capacities for DC electrodes compared to AC electrodes of the same size,[10,11] as mentioned in the introduction.

The situation for large carbon or Søderberg electrodes is quite different. These electrodes have large Biot numbers and correspondingly large internal temperature differences, c.f. Figure 6. Hence, thermal stresses will be the limiting factor, see Section IV.

The value of the Biot number also has other implications. Graphite electrodes with small values of *Bi* have an almost constant temperature throughout their cross sections. This temperature level will be given by the heat balance between the power developed in the electrode and the *average* effect of the conditions at the periphery. Large carbon or Søderberg electrodes with large values of *Bi* instead exhibit a relatively small thermal resistance at the surface. The temperature along the periphery will then be dominated by the *local* ambient temperature and heat-transfer coefficient. Large variations in the ambient conditions along the periphery may then significantly influence the temperature distribution within the electrode.

Similarly, proximity effects can significantly modify the power distribution within an electrode. The influence on the temperature distribution will be small for graphite electrodes (small value of *Bi*), while significant effect is expected for large carbon or Søderberg electrodes (large Biot number).

While our simple model reveals the basic properties and shows how graphite electrodes qualitatively differ from large carbon or Søderberg electrodes, other tools are required to estimate realistic conditions for design and/or operation. We have, for instance, neglected the temperature dependence of the material parameters: the thermal and electrical conductivities, as well as the specific heat capacity, all have a significant temperature dependence. Including the temperature dependence of these parameters will give rise to quantitative changes, but will not significantly change the qualitative results. This also holds true for our other simplifications, such as the omission of nonuniform boundary conditions, vertical heat transport by conduction and advection (slipping), and time transients. A thorough understanding of these effects through numerical simulations is necessary for electrode design and operation, but they lie outside the scope of this work. This work focuses on acquiring a basic understanding of the thermal conditions of the electrode and has used the simplest possible model for this purpose.

The preceding equation analysis has depended on evaluation of nondimensional numbers. Determining the numerical value of these numbers can be a challenge in situations where the material parameters have a significant temperature dependence. When using this model, we recommend using average values that are representative of the expected temperature. In Table II, we have chosen values that are valid at approximately 1000 °C.

The model described in this work is valid when horizontal heat conduction is the main heat-loss mechanism of the electrode. In this regime, numerical simulations will reveal steep, almost vertical, isotherms close to the electrode periphery. We expect this to be the case for the lower part of the electrode.[15] In, and close to, the clamp region, the temperature gradients are very large, and none of the terms in the heat equation can be neglected.[19] Numerical simulations show that the temperature increase from unbaked paste (below 500 °C) to fully baked paste (around 1000 °C) takes place over a vertical distance of only about 25 cm.[15] Due to the importance of small terms in this region, we recommend detailed numerical simulations to understand its scale-up behavior.

VI. CONCLUSIONS

Scale-up of high-current electrodes has been studied using a simple thermal model, which includes the electric power distribution, horizontal heat conduction, and surface heat resistance. The qualitative temperature behavior depends on four nondimensional numbers: the Biot number, which quantifies the relative importance of internal *vs* surface heat-transfer resistance; the squared aspect ratio, which quantifies the relative importance of horizontal and vertical heat conduction; the Péclet number, which quantifies the relative importance of horizontal heat conduction and vertical heat advection; and the relative size of the skin depth, which quantifies the importance of skin effects for alternating currents. For small values of the Biot number (graphite electrodes and small carbon electrodes), the electrode current is limited by the electrode surface temperature. In this case, direct current (DC) electrodes exhibit larger current-carrying capacity than alternating current (AC). For large values of the Biot number (large carbon or Søderberg electrodes), the electrode current is limited by thermal stresses and subsequent breakages due to large temperature differences inside the electrode. In this case, AC electrodes can carry more current than DC electrodes.

ACKNOWLEDGMENTS

This work was supported by the Research Council of Norway under Grant number 247791, and the companies Elkem and Eramet Norway.

FUNDING

Open access funding provided by NORCE Norwegian Research Centre AS.

CONFLICT OF INTEREST

The authors declare that they have no conflict of interest.

VII. APPENDIX

A. *Power Balance*

To evaluate the integral in Eq. [14],

$$q_r = \frac{1}{r}\int_0^r \mathrm{d}r' r' p(r'), \qquad [A1]$$

we need an expression for the power density $p(r)$. The power density is defined as

$$p(r) = \frac{|\mathbf{J}|^2}{\sigma}, \tag{A2}$$

and an expression for $|\mathbf{J}|^2$ is derived in Reference 16 for this geometry:

$$|\mathbf{J}|^2 = \frac{J_{z,\mathrm{DC}}^2 \xi^2}{4} \frac{\mathrm{ber}^2(\xi r/R) + \mathrm{bei}^2(\xi r/R)}{\mathrm{ber}'^2\xi + \mathrm{bei}'^2\xi}. \tag{A3}$$

Here, $\xi = \sqrt{2}R/\delta$ and $J_{z,\mathrm{DC}} = I_{\mathrm{rms}}/\pi R^2$. The functions $\mathrm{ber}\,x$ and $\mathrm{bei}\,x$ are the zeroth-order Kelvin functions, which are defined as[26]

$$\mathrm{ber}\,x + i\,\mathrm{bei}\,x = J_0\left(\frac{1-i}{\sqrt{2}}x\right) \tag{A4}$$

in terms of the zeroth-order Bessel function J_0. Introducing the AC/DC correction factor (Reference 16)

$$\frac{R_{\mathrm{AC}}}{R_{\mathrm{DC}}} = \frac{\xi}{2} \frac{\mathrm{ber}\,\xi\,\mathrm{bei}'\xi - \mathrm{bei}\,\xi\,\mathrm{ber}'\xi}{\mathrm{ber}'^2\xi + \mathrm{bei}'^2\xi}, \tag{A5}$$

this expression can be rewritten as

$$|\mathbf{J}|^2 = \frac{J_{z,\mathrm{DC}}^2 \xi}{2} \frac{R_{\mathrm{AC}}}{R_{\mathrm{DC}}} \frac{\mathrm{ber}^2(\xi r/R) + \mathrm{bei}^2(\xi r/R)}{\mathrm{ber}\,\xi\,\mathrm{bei}'\xi - \mathrm{bei}\,\xi\,\mathrm{ber}'\xi}. \tag{A6}$$

Back-substitution into the equation for q_r and use of the integral substitution $x = \xi r'/R$ and the tabulated integral[26]

$$\int x(\mathrm{ber}^2 x + \mathrm{bei}^2 x)\mathrm{d}x = x(\mathrm{ber}\,x\,\mathrm{bei}'x - \mathrm{bei}\,x\,\mathrm{ber}'x) \tag{A7}$$

gives

$$q_r = \frac{J_{z,\mathrm{DC}}^2 R}{2\sigma} \frac{R_{\mathrm{AC}}}{R_{\mathrm{DC}}} \frac{\beta(\xi r/R)}{\beta(\xi)}, \tag{A8}$$

where we introduced the function

$$\beta(\xi) = \mathrm{ber}\,\xi\,\mathrm{bei}'\xi - \mathrm{bei}\,\xi\,\mathrm{ber}'\xi. \tag{A9}$$

Using the definition of $J_{z,\mathrm{DC}}$, this expression can be rewritten as

$$q_r = \frac{I_{\mathrm{rms}}^2}{2\sigma\pi^2 R^3} \frac{R_{\mathrm{AC}}}{R_{\mathrm{DC}}} \frac{\beta(\xi r/R)}{\beta(\xi)} = \frac{R_{\mathrm{AC}}}{R_{\mathrm{DC}}} g_q(r) q_{R,\mathrm{DC}}, \tag{A10}$$

where we defined

$$g_q(r) = \frac{\beta(\xi r/R)}{\beta(\xi)} \tag{A11}$$

and

$$q_{R,\mathrm{DC}} = \frac{I_{\mathrm{rms}}^2}{2\sigma\pi^2 R^3}. \tag{A12}$$

B. *Temperature Distribution*

The temperature distribution is found by solving Eq. [13]. By reintroducing dimensions and substituting for the integral we evaluated in the previous section, we rewrite Eq. [13] as

$$k\frac{\mathrm{d}T}{\mathrm{d}r} = -\frac{R_{\mathrm{AC}}}{R_{\mathrm{DC}}} \frac{\beta(\xi r/R)}{\beta(\xi)} q_{R,\mathrm{DC}}. \tag{A13}$$

Separation of variables and integration gives

$$T(r) = C - \frac{q_{R,\mathrm{DC}}}{k} \frac{R_{\mathrm{AC}}}{R_{\mathrm{DC}}} \frac{1}{\beta(\xi)} \int_r^R \beta(\xi r'/R)\mathrm{d}r'. \tag{A14}$$

The integration constant C can be determined using the boundary condition in Eq. [12]:

$$\left.\frac{\mathrm{d}T}{\mathrm{d}r}\right|_{r=R} = -\frac{h}{k}[T(R) - T_a]. \tag{A15}$$

We write out the left-hand side of Eq. [A15] using Eq. [A13], and the right-hand side using our solution for $T(r)$ in Eq. [A14], to obtain

$$\frac{R_{\mathrm{AC}}}{R_{\mathrm{DC}}} q_{R,\mathrm{DC}} = h[C - T_a]. \tag{A16}$$

Solving this equation for C gives

$$T(r) = T_a + \frac{1}{h}\frac{R_{\mathrm{AC}}}{R_{\mathrm{DC}}} q_{R,\mathrm{DC}} + \frac{R}{k}\frac{R_{\mathrm{AC}}}{R_{\mathrm{DC}}} q_{R,\mathrm{DC}} \frac{\int_{\xi r/R}^{\xi} \beta(x)\mathrm{d}x}{\xi\beta(\xi)}, \tag{A17}$$

where we used the integral substitution $x = \xi r'/R$. Introducing $\Delta T_{\mathrm{max,DC}} = (Bi/2h) q_{R,\mathrm{DC}}$, and defining

$$g_T(r) = 2\frac{R_{\mathrm{AC}}}{R_{\mathrm{DC}}} \frac{\int_{\xi r/R}^{\xi} \beta(x)\mathrm{d}x}{\xi\beta(\xi)}, \tag{A18}$$

the solution can be rewritten as

$$T(r) = T_a + \frac{2}{Bi}\frac{R_{\mathrm{AC}}}{R_{\mathrm{DC}}} \Delta T_{\mathrm{max,DC}} + g_T(r)\Delta T_{\mathrm{max,DC}} \tag{A19}$$

which can also be written as

$$T(r) = T_a + \Delta T_{\mathrm{surf}} + \Delta T_{\mathrm{int}} \tag{A20}$$

using the definitions in the main text.

C. *DC Limit*

To evaluate these expressions in the DC limit, we use the series expansions of the zeroth-order Kelvin functions around zero[26]:

$$\operatorname{ber} x = 1 - \frac{x^4}{64} + \mathcal{O}(x^8), \qquad [A21]$$

$$\operatorname{ber}' x = -\frac{x^3}{16} + \frac{x^7}{18432} - \mathcal{O}(x^{11}), \qquad [A22]$$

$$\operatorname{bei} x = \frac{x^2}{4} - \frac{x^6}{2304} + \mathcal{O}(x^{10}), \qquad [A23]$$

$$\operatorname{bei}' x = \frac{x}{2} - \frac{x^5}{384} + \mathcal{O}(x^{14}). \qquad [A24]$$

Substitution into Eq. [A9] also gives

$$\beta(x) = \frac{x}{2} + \frac{x^5}{192} + \mathcal{O}(x^9). \qquad [A25]$$

Consequently, for $\xi \ll 1$ the skin effect factor is

$$\frac{R_{AC}}{R_{DC}} = 1 + \frac{\xi^4}{192} - \mathcal{O}(\xi^8). \qquad [A26]$$

Similarly, the shape function g_q is

$$g_q = \frac{r}{R} + \frac{r}{R}\left(\frac{r^4}{R^4} - 1\right)\frac{\xi^4}{96} + \mathcal{O}(\xi^8) \qquad [A27]$$

and the shape function g_T is

$$g_T = 1 - \frac{r^2}{R^2} + \left(1 - \frac{3r^2}{R^2} + \frac{2r^6}{R^6}\right)\frac{\xi^4}{576} + \mathcal{O}(\xi^8). \qquad [A28]$$

As a result, in the DC limit the power integral q_r evaluates to

$$q_r = q_{R,DC} \cdot \left[\frac{r}{R} + \frac{r}{R}\left(\frac{2r^4}{R^4} - 1\right)\frac{\xi^4}{192} + \mathcal{O}(\xi^8)\right], \qquad [A29]$$

and the temperature variation in the interior of the electrode evaluates to

$$\Delta T_{int} = \Delta T_{max,DC} \cdot \left[1 - \frac{r^2}{R^2} + \left(1 - \frac{3r^2}{R^2} + \frac{2r^6}{R^6}\right)\frac{\xi^4}{576} + \mathcal{O}(\xi^8)\right]. \qquad [A30]$$

SUPPLEMENTARY INFORMATION

The online version contains supplementary material available at https://doi.org/10.1007/s11663-023-02811-7.

REFERENCES

1. M. Lackner (ed.): *Scale-Up in Metallurgy*, Verlag ProcessEng Engineering, Wien, 2010.
2. T. McNulty: *Min. Eng.*, 1998, vol. 50(10), pp. 50–55.
3. P.J. Meckey and J.E. Nesset: The impact of commissioning and start-up performance on a mining/metallurgical project. in *Proceedings of the 35th Annual Meeting of Canadian Mineral Processors*, S. Wilson, ed., Canadian Institute of Mining, Metallurgy and Petroleum, Ottawa, Canada, 2003, pp. 331–47.
4. M.W. Kennedy: Electric slag furnace dimensioning. in: *International Smelting Technology Symposium*, J.P. Downey, T.P. Battle, J.F. White, eds., Wiley, Hoboken, 2012, pp. 279–90. https://doi.org/10.1002/9781118364765.ch32.
5. F.V. Andreae: *Trans. Am. Inst. Electr. Eng.*, 1950, vol. 69(1), pp. 557–62. https://doi.org/10.1109/t-aiee.1950.5060186.
6. J. Westly: Critical parameters in design and operation of the submerged-arc furnace. in *Proceedings of the 33th Electric Furnace Conference*, vol. 33. Iron & Steel Society, Houston, 1975, pp. 47–53.
7. J. Westly: Electrode consumption in production of 75% FeSi and Si-met. in *Proceedings of the 42th Electric Furnace Conference*, vol. 42. Iron & Steel Society, Toronto, Canada, 1984, pp. 157–60.
8. A.L. Moolman, M.S. Rennie, and P.J. Brereton-Stiles: Experiences in operation of various electric-arc furnaces under resistance control. in *Infacon IX: International Ferro-Alloy Congress*. South African Institute of Mining and Metallurgy, Quebec City, Canada, 2001, pp. 103–07.
9. N.A. Barcza, I.J. Barker, M.S. Rennie, and P.J. Brereton-Stiles: The application and scale-up of AC and DC smelting furnaces for ferro-alloys. in *60th Electric Furnace Conference Proceedings*. Iron & Steel Society, Warrendale, 2002, pp. 425–37.
10. GrafTech International: UCAR Graphite Electrodes. http://s2.q4cdn.com/282965219/files/doc_downloads/customer/UCAR-Graphite-Electrodes-Brochure-Web.pdf, 2005.
11. SGL Group: Ultra-High-Performance Graphite Electrodes. https://d3pcsg2wjq9izr.cloudfront.net/files/34597/download/669746/Graphite_electrodes_e.pdf, 2014.
12. R. Innvær, K. Fidje, and R. Ugland: Effect of current variations on material properties and thermal stresses in Søderberg electrodes. in *Proceedings of the 4th International Ferro-Alloys Congress (INFACON IV)*. South African Institute of Mining and Metallurgy, Rio de Janeiro, Brazil, 1986, pp. 321–30.
13. R. Innvær: A status for the Søderberg smelting electrode. in *Proceedings of the XIIth Congress of the International Union for Electroheat*, Montreal, Canada, 1992, pp. 44–53.
14. C. Mathy, J. Borlée, and M. Wauters: Monitoring System for Controlling and Reducing the Electrode Consumption in DC EAF Plants. EUR Research Fund for Coal and Steel, vol. 23889. Office for Official Publications of the European Communities, Luxembourg, 2009.
15. B. Larsen, H. Feldborg, and S.A. Halvorsen: Minimizing thermal stress during shutdown of Søderberg electrodes. in *Proceedings of the 13th International Ferro-Alloys Congress (INFACON XIII). South African Institute of Mining and Metallurgy*, Almaty, Kazakhstan, 2013, pp. 453–66.
16. E.V. Herland, M. Sparta, and S.A. Halvorsen: *Metall. Mater. Trans. B*, 2019, vol. 50B, pp. 2884–97. https://doi.org/10.1007/s11663-019-01651-8.
17. S. Ramo, J.R. Whinnery, and T. Van Duzer: *Fields and Waves in Communication Electronics*, 3rd ed., Wiley, New York, 1994.
18. G.S. Smith: *Eur. J. Phys.*, 2014, vol. 35(2), p. 025002. https://doi.org/10.1088/0143-0807/35/2/025002.
19. S.A. Halvorsen, A.M. Valderhaug, and J. Fors: Basic properties of the Persson type composite electrode. in *Proceedings of the 57th Electric Furnace Conference*, vol. 57. Iron & Steel Society, Pittsburgh, 1999.
20. F.P. Incropera, D.P. DeWitt, T.L. Bergman, and A.S. Lavine: *Fundamentals of Heat and Mass Transfer*, 6th ed., Wiley, Hoboken, 2007.

21. M.J.O. Strutt: *Lond. Edinb. Dublin Philos. Mag. J. Sci.*, 1928, vol. 5(31), pp. 904–14. https://doi.org/10.1080/14786440508564533.
22. A. Jordan, A. Szybiak, M. Benmouna, and A. Barka: *Int. J. Heat Mass Transf.*, 1987, vol. 30(7), pp. 1539–41. https://doi.org/10.1016/0017-9310(87)90185-2.
23. A. Barletta, and E. Zanchini: *Wärme- und Stoffübertragung*, 1994, vol. 29(5), pp. 285–90. https://doi.org/10.1007/BF01578412.
24. L.D. Landau, and E.M. Lifshitz: *Theory of Elasticity, Course of Theoretical Physics*, vol. 7, 2nd ed., Pergamon Press, Oxford, 1970.
25. M. Fromreide, D. Gómez, S.A. Halvorsen, E.V. Herland, and P. Salgado: *Appl. Math. Model.*, 2021, vol. 98, pp. 59–70. https://doi.org/10.1016/j.apm.2021.04.034.
26. M. Abramowitz, and I.A. Stegun: *Handbook of Mathematical Functions with Formulas, Graphs, and Mathematical Tables*, 10th edn. Applied Mathematics Series, vol. 55. National Bureau of Standards, Washington, 1972.